

Prediction of Demands on Non-Structural Components in Base-Isolated Structures

K. Haymes, T.J. Sullivan & R. Chandramohan

University of Canterbury, Department of Civil and Natural Resources Engineering, Christchurch.

L. Wiebe

McMaster University, Department of Civil Engineering, Hamilton, Ontario.

ABSTRACT

This study examines seismic demands imposed on non-structural components within base isolated structures. Although several previous studies have focussed on the ability of base isolators to limit structural damage, very few have predicted their influence on the demands imposed on acceleration-sensitive non-structural components. Hence, the motivation of this study is to progress towards an improved design philosophy for non-structural components located within base-isolated structures.

The dynamic response of base-isolated structures is studied using simple two-degree-of-freedom models that describe the motion of the isolator and the superstructure. Bilinear hysteretic models are used to represent the behaviour of flat slider and elastomeric bearing isolators, while the superstructure is assumed to remain elastic. The results of the numerical simulations are used to relate isolator, superstructure, and ground motion characteristics to the observed floor response spectra. Special consideration is given to higher mode responses, which can produce significant demands on non-structural elements. The results will inform a prediction approach that is in development that aims to be more accurate than current international non-structural design practices, without compromising on simplicity, thus facilitating its adoption in practical design applications.

1 INTRODUCTION

The objective of this work is to provide a robust empirical basis for a prediction framework that will extend a method recently developed by the authors to predict elastic floor response spectra of fixed-base structures (Haymes et al., 2020) by incorporating the influence of the nonlinear base-isolator response. This work is motivated by focus on improving performance of non-structural components by accurately and easily predicting seismic demands acting upon them.

Base isolation can be an effective means to reduce the seismic demands on the superstructure that it may otherwise experience if it were fixed at the base. Following the damage and disruption of the Canterbury earthquakes there has been a proliferation of base isolated structures constructed in Christchurch driven by an increase in the awareness of building owners and tenants of the potential improvement of the seismic performance that base isolation can offer (Keen et al., 2016). Base isolation concentrates the nonlinear response of the structural system in the isolators, therefore reducing floor accelerations of the superstructure, and intuitively reducing the demands on acceleration-sensitive non-structural elements. The frequency content and amplitude of these demands are altered by the nonlinearity at the base of the structure, however, resulting in complex dynamic responses of the non-structural components which may be difficult to quantify.

The prediction of seismic demands on non-structural components using nonlinear time history analysis is complex and requires many engineering judgements that may be difficult to verify in base isolated systems. Instead, designers may use the peak response of non-structural components based on their vibrational characteristics given by floor response spectra. These can be directly estimated using modal superposition. Current approaches for multi-degree-of-freedom (MDOF) fixed base structures (Haymes et al., 2020; Kehoe & Hachem, 2003; Vukobratović & Fajfar, 2016; Welch & Sullivan, 2017) cannot be applied for base isolated structures in their current forms. The method by Zuniga-Cuevas & Teran-Gilmore (2013) is limited to cases where the superstructural stiffness is significantly greater than that of the isolators, and makes no provision for the influence of higher structural modes which have been observed to be significant (Anajafi et al., 2020; Calvi & Ruggiero, 2017) particularly as many non-structural components respond with short periods (Applied Technology Council, 2018).

This work investigates the characteristics of floor acceleration response spectra in base isolated structures by examining the results of numerical simulations of two-degree-of-freedom (2DOF) lumped mass stick models with lead plug bearing (LPB) and flat slider bearing (FSB) isolators. Figure 1 illustrates the 2DOF representation of the MDOF base isolated system. The superstructure is reduced to a single-degree-of-freedom (SDOF) with lumped mass m_{str} and stiffness k_{str} , attached to the mass at the base, m_{iso} , with the isolator stiffness, k_{iso} , represented by a bilinear force-displacement backbone curve shown in Figure 1b with initial stiffness $k_{init,iso}$, tangent stiffness $k_{tang,iso}$, and secant stiffness $k_{secant,iso}$. The framework developed herein considers the mass ratio, m_{iso}/m_{str} , which remain constant during an earthquake; and stiffness ratio, k_{iso}/k_{str} , which reduces during an earthquake from the initial isolator stiffness to the secant stiffness. The properties of an eight-storey base isolated structure in Christchurch, New Zealand, are adopted herein to provide realistic representative values for analysis, derived from the work by Yang et al. (2020).

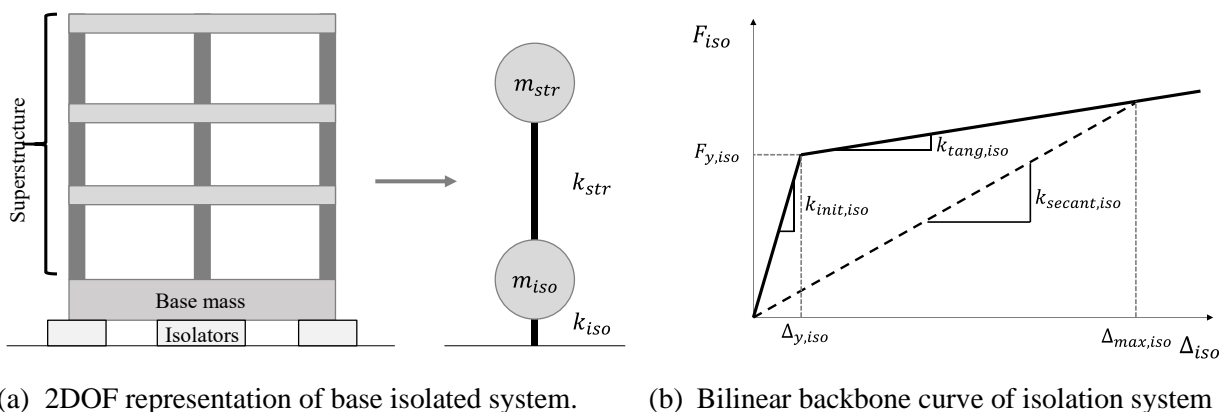


Figure 1: A multi-storey base isolated structure modelled as a two-degree-of-freedom (2DOF) system and the backbone curve of the isolation system.

2 IDEALISATION OF BASE ISOLATION SYSTEM AS 2DOF

The expected modal response of base isolated structures is often characterised using two SDOF systems: a fixed base SDOF of the superstructure; or a rigid body superstructural response with superstructural and base masses lumped at the top of the isolators (Kelly, 1990). The latter was adopted in the method by Zuniga-Cuevas & Teran-Gilmore (2013). A 2DOF representation of base isolated structures may better prescribe the vibrational behaviours observed in floor response spectra, however. Figure 2 shows the first mode period computed from these models, T_{SDOF} , compared to that computed using a 2DOF representation, $T_{1,2DOF}$, for a range of ratios of the stiffnesses and masses of the isolators to superstructure. The stiffness and mass ratios for the case study structure are indicated where the vertical orange (LPB) and purple (FSB) lines intersect the green curve. The SDOF systems only provide accurate estimates when the isolator stiffness is either far greater or smaller than that of the superstructure. In consequence the lead-plug bearing, with a similar stiffness to the superstructure, is poorly represented by both SDOF models. This result supports the consideration of the full 2DOF system and mass and stiffness ratios for characterisation of the modal responses that influence floor response spectra.

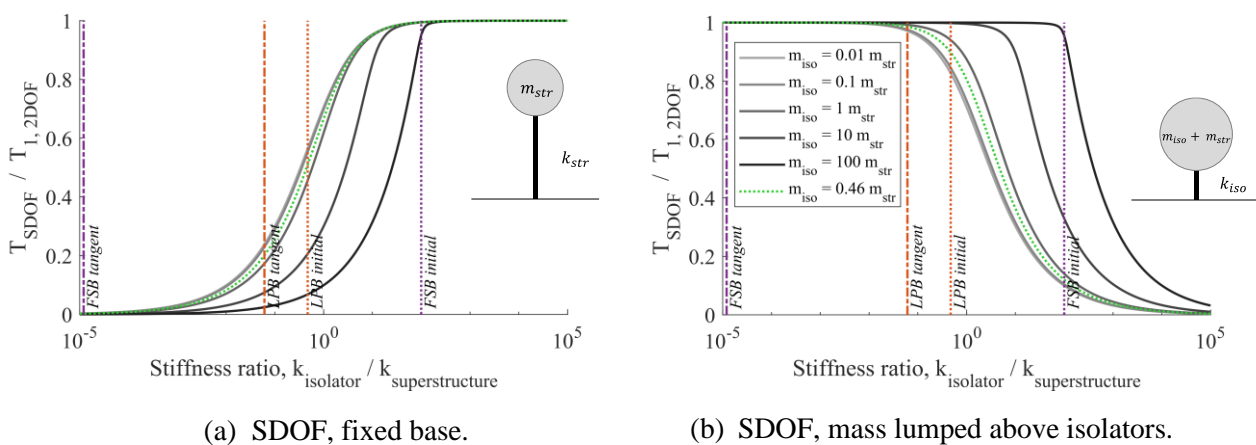


Figure 2: First mode period of SDOF models of the isolated structure compared to that computed using the corresponding 2DOF representation for a range of ratios of the isolation to superstructural stiffnesses and masses. The case-study stiffness and mass ratios ($m_{ratio} = 0.46$) are indicated.

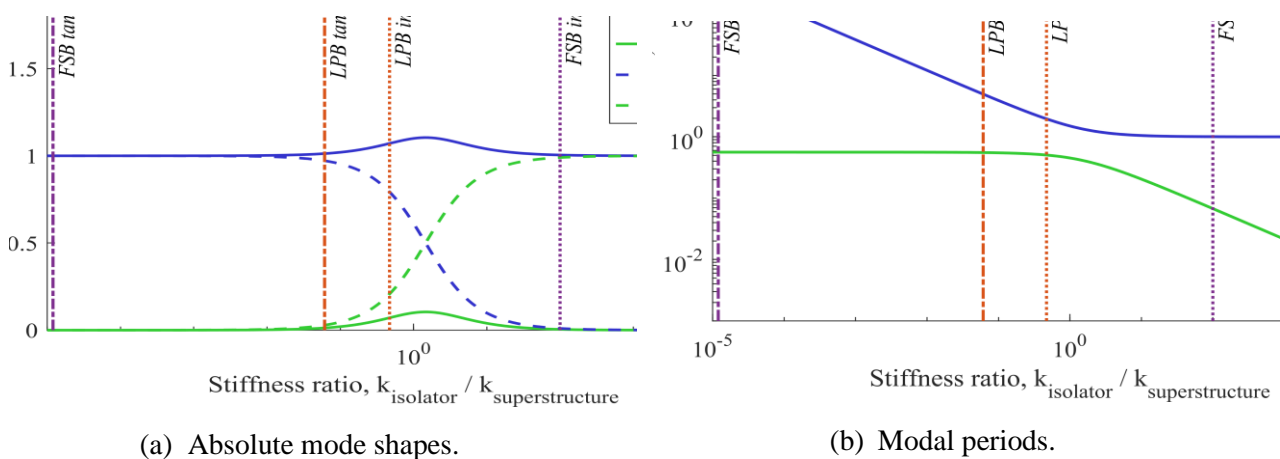


Figure 3: Mode shapes and modal periods for a range of ratios of the isolation to superstructural stiffnesses with for the case study where the base mass is equal to 0.46 of the superstructural mass. The stiffness ratios associated with the initial and tangent isolator stiffnesses are indicated.

Prediction of floor response spectra using modal superposition requires the mode shapes and periods of the structure supporting the non-structural component. Figure 3 shows the absolute values of the first and second mode shapes (a) and periods (b) using the case-study masses and the ratio of the stiffness of the initial and tangent post-yield stiffnesses of the isolators to the superstructural stiffness as upper and lower bounds of modal responses. In Figure 3b the modal periods are normalised by the first mode period of the highest stiffness ratio, for which the 2DOF is essentially a fixed base structure as in Figure 2a. Figure 3 shows that at a very high stiffness ratio, the superstructure responds as if it is fixed base in the first mode, with the base mass oscillating with a very short period in the second mode and the superstructural mass remaining stationary. As the stiffness ratio decreases, the superstructural response increases to a peak value in both modes and the response of the base mass shifts from the second mode to the first. The periods of both modes elongate. At the very low stiffness ratios, the first mode acts as a rigid body, as in the lumped SDOF, with an ever elongating period. In the second mode the response of both masses tends to zero and the period plateaus.

3 FLOOR ACCELERATION RESPONSE SPECTRA

Nonlinear time-history analyses using 2DOF models of the case-study structure were conducted using OpenSees (McKenna Fenves et al., 2000). The lead plug bearing isolators were modelled using the “elastomericBearingPlasticity” element (Schellenberg, 2016) and the flat slider bearings were modelled using the “flatSliderBearing” element (Schellenberg, 2014).

The periods of the two modes on the 2DOF models were computed using eigenvalue analysis adopting the initial and tangent post-yield isolator stiffnesses and are given in Table 1. Secant periods were similarly computed using the secant isolator stiffnesses, given as the maximum base shear and isolator displacements.

The time history analyses were conducted to achieve four target displacements, and therefore secant first mode periods, using 20 ground motions corresponding to a hazard with return period of approximately one in 2475 years (Yeow et al. 2018). The mode shapes using initial, tangent, and secant isolator stiffnesses are given in Figure 4. The median acceleration response spectra for each suite of 20 motions at each intensity corresponding to a target period, computed at the ground level, the isolator mass, and the superstructural mass for the lead plug bearing and flat slider bearing isolators are shown in Figures 5 and 6, respectively.

Table 1: 2DOF modal periods computed using initial and tangent post-yield stiffnesses of the lead plug bearing and flat slider bearing isolators.

	$T_{1,initial}$	$T_{1,tangent}$	$T_{2,initial}$	$T_{2,tangent}$
Lead rubber bearing	1.20 s	3.03 s	0.31 s	0.34 s
Flat slider bearing	0.61 s	233 s	0.04 s	0.34 s

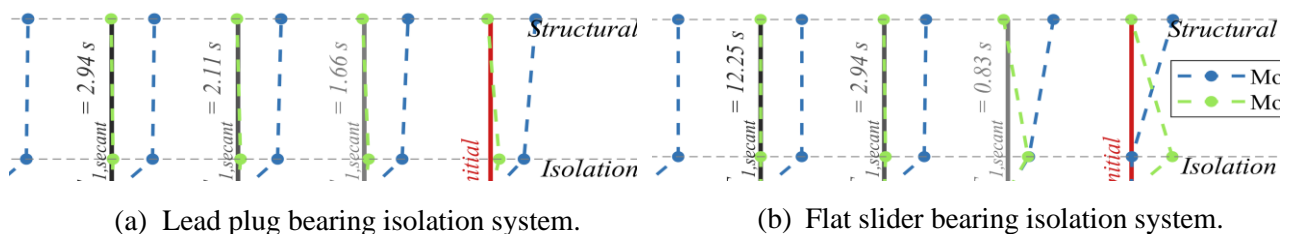
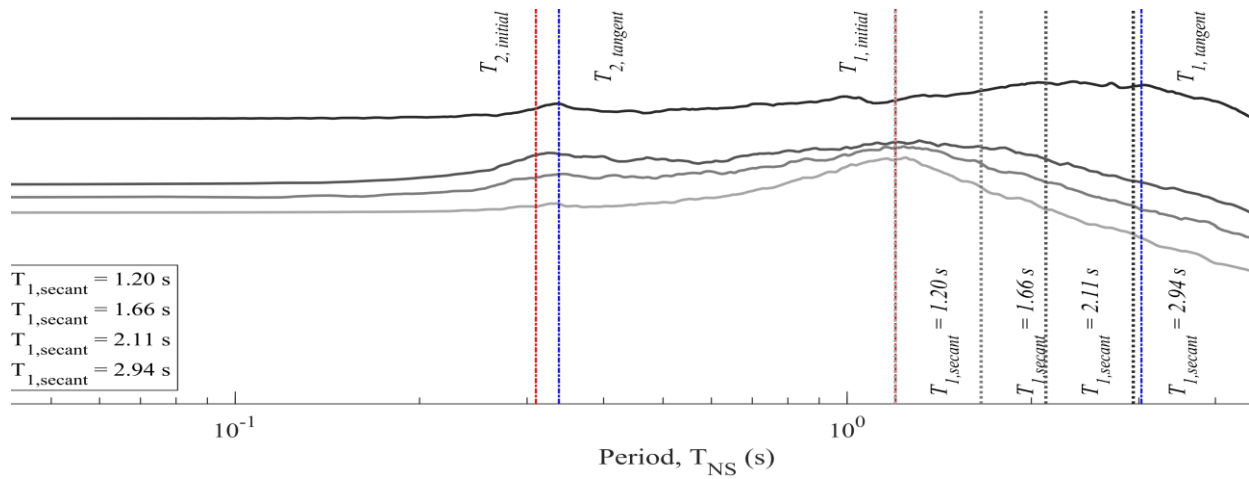
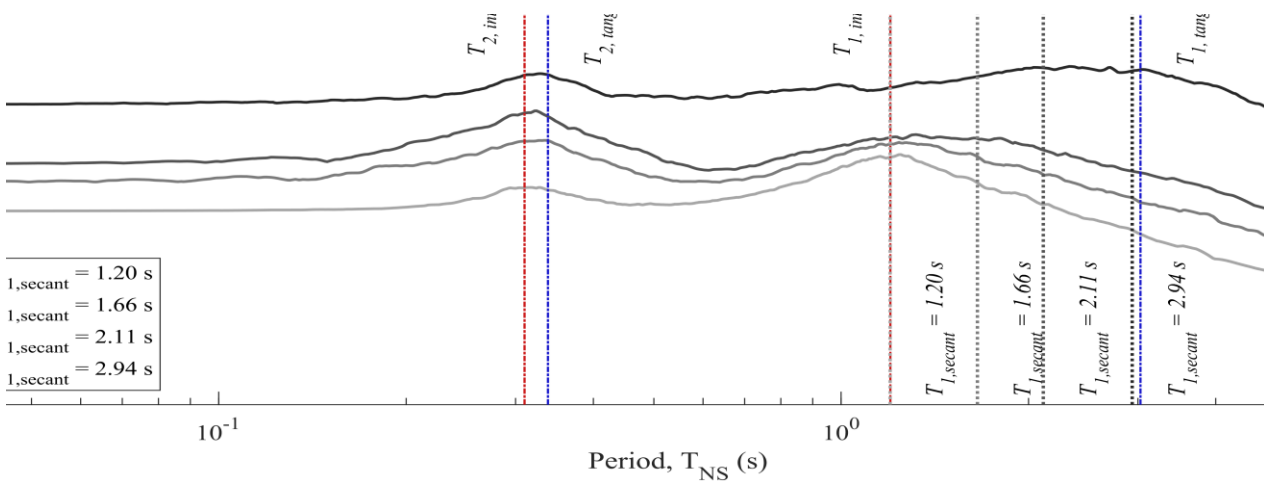


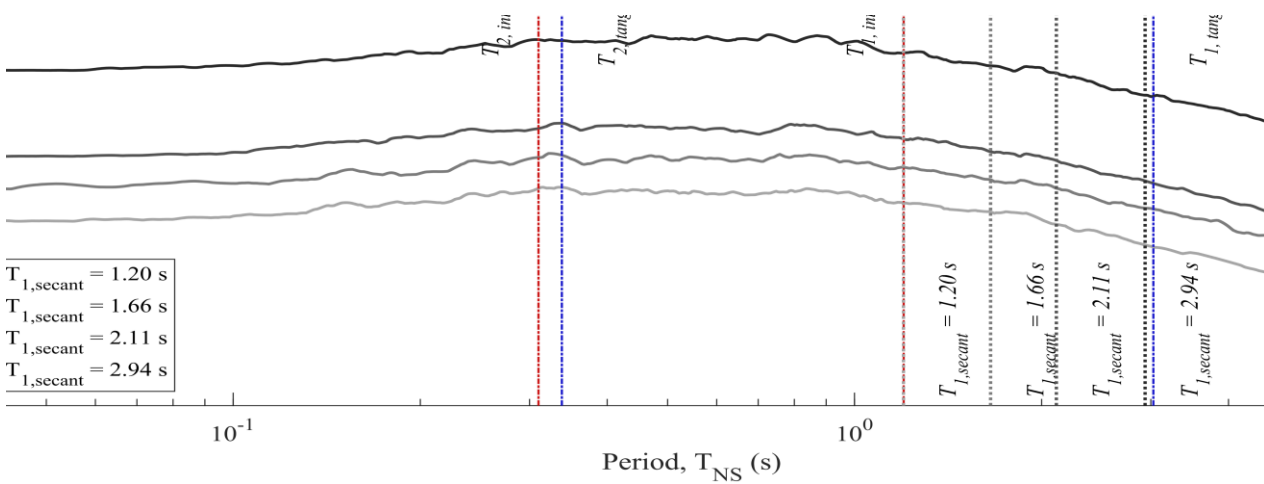
Figure 4: Mode shapes computed using 2DOF models with the isolator adopting the initial, target, and tangent stiffnesses for the lead plug and flat slider bearing isolation systems.



(a) Superstructural level.

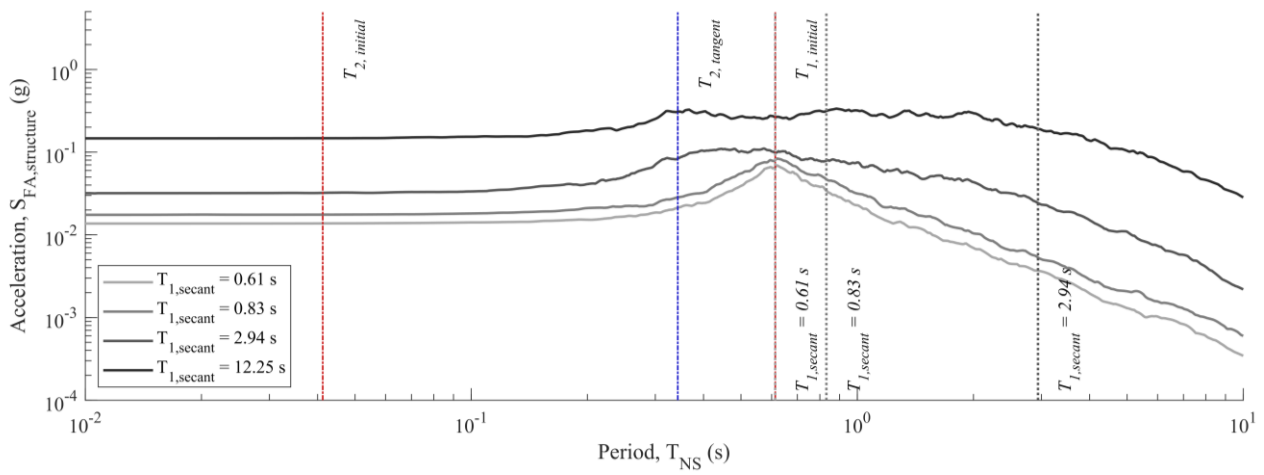


(b) Base mass level.

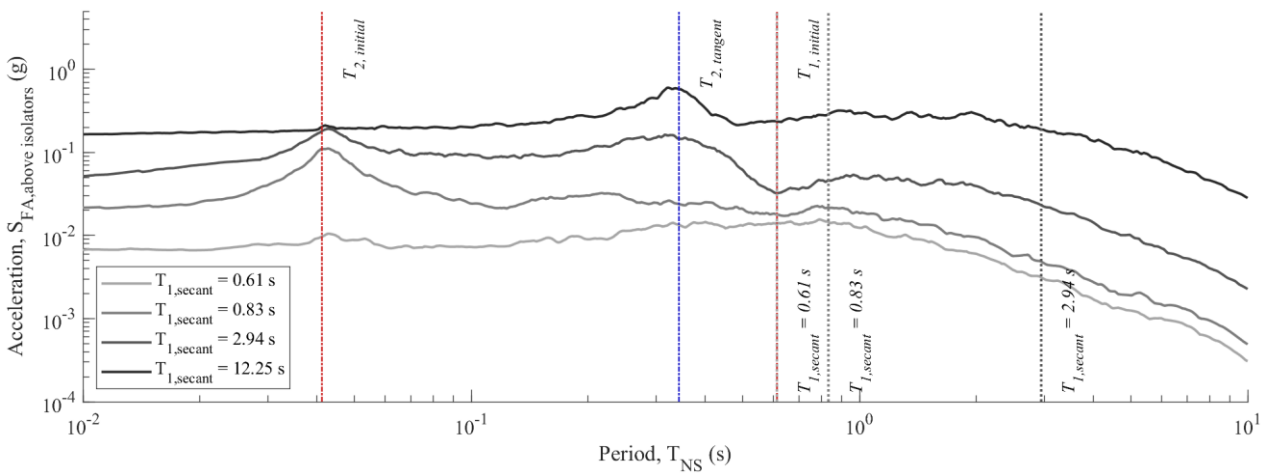


(c) Ground.

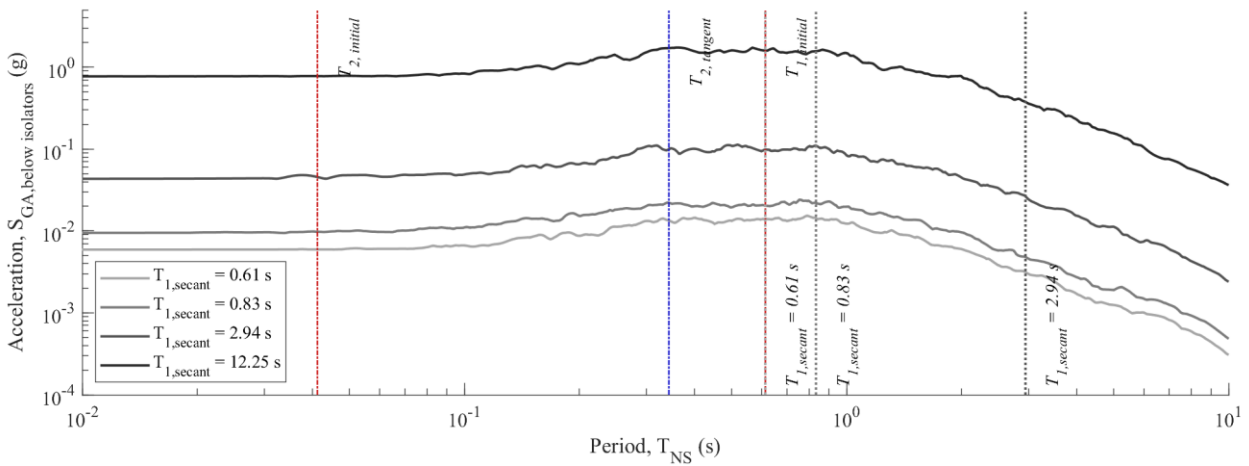
Figure 5: Median floor acceleration response spectra computed from 20 records at 4 target displacements using time-history analyses of the 2DOF system with lead plug bearing isolators.



(a) Superstructural level.



(b) Base mass level.



(c) Ground.

Figure 6: Median floor acceleration response spectra computed from 20 records at 4 target displacements using time-history analyses of the 2DOF system with flat slider bearing isolators.

4 DISCUSSION

The first period computed through eigenvalue analysis of the 2DOF system using the secant stiffness of the isolators appears to be a good measure from which to characterise inelastic response. Increasing peak isolator displacement corresponds to reduction of the amplification of the ground motion observed in both the superstructural and base masses in both Figures 5 and 6. At non-structural periods greater than the secant first mode period, however, the ground motion appears to be transmitted directly to the floors unaltered.

There are distinct amplification peaks at the initial modal periods that are distributed between the masses as expected by the corresponding mode shapes that are shown in Figure 4. This is most pronounced in the flat slider bearing spectra where amplification is observed in the initial first mode at the superstructural mass and not the base mass, whereas only the base mass amplifies the accelerations in the initial second mode. This amplification is lower than that predicted using the elastic provisions in Haymes et al. (2020), suggesting that prediction provisions could include reduction factors tuned to each mode and isolator backbone curve.

The amplification of the spectral ordinates between the initial and secant first periods also appear to follow the rigid body shape as inelasticity increases, as both base and superstructural levels exhibit similar accelerations. The plateau of demands in this region does not extend as far as the secant period. This may be due to the isolator only displacing to this maximum once which does not allow the non-structural components with these periods to resonate with this degree of inelastic response over multiple cycles. The secant first mode period may act as an upper bound for prediction provisions.

Figure 3b shows that the period of the second mode approaches a near constant value with a decreasing stiffness ratio of the isolation to superstructural stiffnesses. This corresponds to the relatively minor elongation from the the initial to the tangent second modal periods in the lead plug bearing spectra in Figure 5, and the greater elongation of the periods in the flat slider bearing spectra in Figure 6. There is significant amplification observed near the second mode periods computed using the tangent post-yield isolator stiffnesses in both Figures 5 and 6 at most inelastic target displacements. This may support simply using the tangent second mode period for prediction provisions. This amplification is not anticipated by the corresponding mode shapes, shown in Figure 4, which tend to zero as the peak isolator displacement increases. This is driven by the modal participation factor approaching zero.

5 CONCLUSIONS

The dynamic response of base-isolated structures was studied using simple two-degree-of-freedom models. Bilinear hysteretic models representative of the behaviour of flat slider and lead plug bearing isolators were adopted and time-history analyses were conducted with a suite of 20 ground motions scaled to produce target isolator maximum displacements. Modal properties were examined for a range of stiffnesses and masses of the superstructure and isolators and related to observations of floor acceleration response spectra.

The mode shapes and periods of the first and second modes computed using eigenvalue analysis of the 2DOF system with initial and inelastic base isolator stiffnesses were observed to directly correspond to amplifications of the floor response spectra.

These results will inform a prediction approach that is in development that aims to be more accurate than current international non-structural design practices, without compromising on simplicity, thus facilitating its adoption in practical design applications.

6 ACKNOWLEDGEMENTS

This project was (partially) supported by QuakeCoRE, a New Zealand Tertiary Education Commission-funded Centre.

7 REFERENCES

- Anajafi, H., Medina, R. A., & Santini-Bell, E. (2020). Effects of the improper modeling of viscous damping on the first-mode and higher-mode dominated responses of base-isolated buildings. *Earthquake Engineering & Structural Dynamics*, 49(1), 51–73. <https://doi.org/10.1002/eqe.3223>
- Applied Technology Council. (2018). *Recommendations for improved seismic performance of nonstructural components*. <https://doi.org/10.6028/NIST.GCR.18-917-43>
- Calvi, P. M., & Ruggiero, D. M. (2017). Earthquake-induced floor accelerations in base isolated structures. *16th World Conference on Earthquake Engineering*.
- Haymes, K., Sullivan, T., & Chandramohan, R. (2020). A practice-oriented method for estimating elastic floor response spectra. *Bulletin of the New Zealand Society for Earthquake Engineering*, 53(3), 116–136. <https://doi.org/10.5459/bnzsee.53.3.116-136>
- Keen, J. M., Yuen, K. W., & Whittaker, D. (2016). Seismic isolation design during the Christchurch Rebuild - Practitioner's challenges in the absence of a New Zealand standard. *New Zealand Society for Earthquake Engineering Annual Technical Conference*.
- Kehoe, B. E., & Hachem, M. (2003, January 1). Procedures for Estimating Floor Accelerations. *ATC-29-2 Seminar on Seismic Design, Performance, and Retrofit of Nonstructural Components in Critical Facilities*.
- Kelly, J. M. (1990). Base Isolation: Linear Theory and Design. *Earthquake Spectra*, 6(2), 223–244. <https://doi.org/10.1193/1.1585566>
- McKenna Fenves, G. L., Scott, M. H., & Jeremić, B., F. (2000). *Open system for earthquake engineering simulation (OpenSees)* <http://opensees.berkeley.edu>. <http://opensees.berkeley.edu>
- Schellenberg, A. (2014). *Flat Slider Bearing Element*. https://opensees.berkeley.edu/wiki/index.php/Flat_Slider_Bearing_Element
- Schellenberg, A. (2016). *Elastomeric Bearing (Plasticity) Element*. [opensees.berkeley.edu/wiki/index.php/Elastomeric_Bearing_\(Plasticity\)_Element](https://opensees.berkeley.edu/wiki/index.php/Elastomeric_Bearing_(Plasticity)_Element)
- Vukobratović, V., & Fajfar, P. (2016). A method for the direct estimation of floor acceleration spectra for elastic and inelastic MDOF structures. *Earthquake Engineering & Structural Dynamics*, 45(15), 2495–2511. <https://doi.org/10.1002/eqe.2779>
- Welch, D. P., & Sullivan, T. J. (2017). Illustrating a new possibility for the estimation of floor spectra in nonlinear multi-degree of freedom systems. *16th World Conference on Earthquake Engineering*.
- Yang, A., Sullivan, T. J., Bradley, B. A., & Pettinga, D. J. (2020). *Seismic Performance Assessment of a Base Isolated Building*. University of Canterbury.
- Yeow, T. Z., Orumiyehi, A., Sullivan, T. J., MacRae, G. A., Clifton, G. C., & Elwood, K. J. (2018). Seismic performance of steel friction connections considering direct-repair costs. *Bulletin of Earthquake Engineering*, 16(12), 5963–5993. <https://doi.org/10.1007/s10518-018-0421-x>
- Zuniga-Cuevas, O., & Teran-Gilmore, A. (2013). Parametric study on acceleration-based design of low-rise base isolated systems. *Engineering Structures*, 53, 25–37. <https://doi.org/10.1016/j.engstruct.2013.03.012>